

Positron annihilation and electron correlations in metals*

D. N. Lowy[†] and A. D. Jackson

Physics Department, State University of New York at Stony Brook, Stony Brook, New York 11794

(Received 3 February 1975)

The annihilation rate of positrons in metals can be related to the correlated electron wave function at the positron site. It is argued that the effective interaction at short distance for a positron in an electron gas should be dominated by terms involving one and two electrons. The positron-electron wave function is thus calculated using an effective interaction which includes the strong screening effects from one highly correlated screening electron. The electron wave functions are approximately antisymmetrized using the analogy of a recoilless impurity. The positron annihilation rates calculated using this wave function are in good agreement with the observed rates over the whole range of electron densities found in alkali metals.

I. INTRODUCTION

In a previous paper¹ (referred to as LB) a scheme was developed for calculating the effective interaction in a pure electron gas. In this paper we extend the method to the problem of a positron impurity in the electron gas. The positron has been used extensively as a probe to measure electron structure in metals and to measure the electron structure of defects in metals.² It is therefore important to have a good understanding of how positrons interact with electrons in a many-electron medium. In particular, we would like to construct the effective electron-positron interaction at short distances and use it to calculate the positron annihilation rate in the electron gas at metallic densities.

In experimental measurements of positron annihilations in metals, the positron is introduced into the metal from a source (e.g., ²²Na) embedded in the metal.³ The ²²Na nucleus undergoes β^+ decay with the emission of a 1.28-MeV γ ray. The annihilation of the positron with an electron in the metal results in the emission of two 0.51-MeV γ rays in nearly opposite directions. Ferrell⁴ showed that the annihilation rate R is proportional to the electron density at the positron site, averaged over all positron sites:

$$R = \frac{1}{4} [R_{ps} / |\Phi_{ps}(0)|^2] \times \int d^3r \langle 0 | \psi_{\pm}^*(\vec{r}) \psi_{\pm}(\vec{r}) \psi_{\pm}^*(\vec{r}) \psi_{\pm}(\vec{r}) | 0 \rangle, \quad (1)$$

where $\psi_{\pm}(\vec{r})$ are the second quantized operators for the positron and electron fields, R_{ps} is the annihilation rate of positronium, and $\Phi_{ps}(\vec{r})$ is the positronium wave function. The positron-electron interactions within the metal are strong, as shown by the observed annihilation rates which are an order of magnitude greater than would be

expected for a noninteracting test particle (Fig. 1). At room temperature a positron thermalizes 10^{-12} to 10^{-11} sec after it enters the metal.^{5,6}

This is much shorter than its average lifetime of more than 10^{-10} sec. The annihilating positron may therefore be taken to be in its lowest-energy Bloch wave function for the lattice potential. This lowest-energy Bloch wave will avoid the positively charged ion cores, and since the core electrons for the alkali metals are tightly bound to their ions, the positron should mainly annihilate with the valence electrons which are free to accumulate around the positron. Since the annihilation rate depends only on the electron density at the positron site, the electron gas should be a satisfactory model for annihilations with valence electrons.

Ferrell⁴ proposed calculating the electron density using a perturbation expansion of the screened Coulomb interaction between the positron and electron, but Kahana⁷ showed that such finite-order expansions could not produce sufficient buildup of electron density around the positron to account for the observed rates. Kahana proposed summing the infinite set of ladder diagrams for a static screened interaction using the Bethe-Goldstone equation. For the higher electron densities $r_s \leq 4$, his results agreed remarkably well with experiment (Fig. 1). In subsequent papers, Carbotte and Kahana examined various modifications to this method such as introducing one nonstatic screened interaction,⁸ inserting low-order self-energy terms,⁸ or adding diagrams needed to satisfy the charge sum rule,⁹ which Bergersen⁹ had shown was violated in the original Kahana formulation.⁷ In all cases little effect was seen on positron lifetimes. Kahana⁷ also evaluated the plasmon contribution to the electron buildup near the positron with the assumption that the $e^- - e^+$ interaction through the plasmon does not depend on their momentum. He found that the plasmon contribution

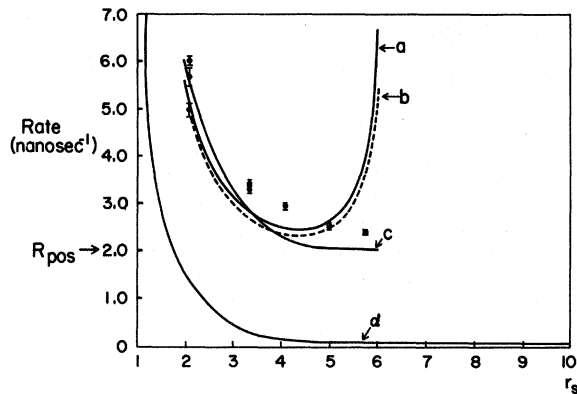


FIG. 1. Positron-annihilation rates in nsec^{-1} . Experimental annihilation rates are taken from Refs. 30–35. Curve (a) is Kahana's (Ref. 7) results extended to lower density. Curve (b) is Sjölander and Stott's (Ref. 18) results using a two-component STLS theory. Curve (c) is Bhattacharyya and Singwi's (Ref. 19) results using STLS theory, but with additional three-body terms. Note their rate at low densities. Curve (d) shows the rates predicted if we neglect the positron attraction.

was small for metallic densities. Further modifications and corrections have been suggested by other authors. Alternative static interactions have been used by Zuchelli and Hickman,¹⁰ by Crowell *et al.*¹¹ and by Arponen and Jauho.¹² They all obtain rates similar to those of Kahana. Kanazawa *et al.*,¹³ Crowell *et al.*,¹¹ and Arponen and Jauho¹² have examined corrections to the ladder sum arising from particle-hole interactions. These additions produce only minor corrections to the original Kahana results. The Bethe-Goldstone equation plays a central role in these calculations, and a common feature of all of them is that their rates diverge when the density decreases below $r_s \approx 4$. At $r_s = 6$ the Bethe-Goldstone rates are about three times the rate observed for cesium, and at slightly lower densities the calculated Bethe-Goldstone rates go to infinity (see Fig. 1). The Bethe-Goldstone equation relies on a Pauli projection operator acting on the intermediate electron states to approximate the antisymmetry of the N -electron wave function. In Sec. III we examine the validity of this approximation. Because of certain important classes of three-body terms the approximation is in fact not valid for this particular problem; hence, the Bethe-Goldstone equation does not give the correct positron-electron wave function. We show in Sec. IV that this inappropriate use of the Pauli operator leads to unphysical bound states embedded in the continuum at positive energies and that the low-density divergence in the Bethe-Goldstone rates is the result of using an incorrect plane-wave nor-

malization for these bound states. We find that at densities higher than $r_s = 4$ the poles do not seriously affect the numerical results.

Hede and Carbotte¹⁴ and Carbotte and Salvadori¹⁵ have generalized the electron-gas theories to provide a better description of positron annihilation in real metals. Hede and Carbotte modified the ladder approximation to include low-order electron-lattice interactions. The main effect of the periodic-lattice potential is the introduction of momentum components $\vec{k} + \vec{G}$ into the unexcited-electron wave functions of wave vector $|\vec{k}| < k_F$, where \vec{G} is a reciprocal-lattice vector. This enhances the contribution to the annihilation rate from high-momentum electrons, but the change in the total rate is small. Annihilation rates from core electrons have been calculated in the ladder approximation by Carbotte and Salvadori. A generalization of the electron-gas theory by Carbotte¹⁵ enables the Bloch nature of the particle states to be included. The ladder sum of Coulomb interactions between the positron and a core electron is calculated assuming that the intermediate electron states are all conduction-band Bloch states. Carbotte and Salvadori estimate that the contribution to the annihilation rate from core electrons is about 15% of the total rate for sodium and about 20% for aluminum.

West¹⁶ has estimated separate core- and valence-electron contributions to the total rate on the basis of angular distribution data for the 0.511-MeV γ rays. Annihilation of a stationary positron with an unexcited valence electron leads to a parabolic angular distribution centered at $\theta = \pi$ with a width of ~ 4 mrad. Annihilation with core electrons leads to broader angular distributions due to high-momentum components in the electron bound-state wave function. West fitted these tails with a Gaussian shape. The annihilation rate for valence electrons alone is readily calculated in terms of the areas of the Gaussian and parabolic components of the angular distributions (A_G and A_p , respectively) and the observed rate R as

$$R_{\text{val}} = \frac{R}{1 + A_G/A_p}. \quad (2)$$

Using Eq. (2) and West's values for A_G and A_p , the values for R_{val} are far below Kahana's curve: for potassium R_{val} is 1.8 nsec^{-1} , for sodium 1.9 nsec^{-1} , for lithium 2.3 nsec^{-1} , and for aluminum 5.0 nsec^{-1} . Note that West's analysis in terms of an effective valence-electron density relies heavily on the assumption, valid in the noninteracting case, that $R \propto (r_s)^{-3}$. This is not a good approximation either to Kahana's calculated rates or the experimental annihilation rates as a function of r_s .

The center-of-mass momentum of the annihilating $e^+ - e^-$ pair can be measured more directly by determining the Doppler shift of the γ rays. This technique is insensitive to possible elastic scattering of the γ rays. Such measurements have recently been made by Geisler, Lynn, and Golland.¹⁷ Preliminary results indicate that the high-momentum tails are significantly different from those observed in angular-distribution measurements. One would like to see an experiment carried out which directly determines just how much the scattering of the γ rays inside the sample affects the resolution in angular-distribution experiments. When more complete data from the Geisler *et al.* experiment is available, it will be interesting to use the data to recalculate R_{val} .

A quite different approach to the problem of calculating the annihilation rate has been used by Sjölander and Stott¹⁸ and by Bhattacharyya and Singwi.¹⁹ They have developed suitably modified versions of the Singwi, Tosi, Land, and Sjölander (STLS) electron-gas theory.²⁰ Sjölander and Stott expanded the theory for a two-component (positron-electron) system, and then took the limit of zero positron density. They calculated a positron-electron correlation function from which they could obtain annihilation rates for a given electron density. Their computed rates are in striking agreement with those of Kahana and, like Kahana's, diverge at low densities (Fig. 1). Bhattacharyya and Singwi employ Vashishta and Singwi's²¹ modification of the STLS theory. Vashishta and Singwi allow for changes in the pair-correlation function in a weak external field by adding a term to the STLS local-field correction which involves the density derivative of the equilibrium pair-correlation function. Since this derivative is related to the three-body equilibrium correlation function, certain three-body correlations have been built in. Looking ahead to our conclusions in Secs. II and III regarding the importance of some three-body terms and the inapplicability of the Bethe-Goldstone equation to this problem, it is interesting that Bhattacharyya and Singwi found that their three-body modifications (i) altered the effective interaction only for small momentum transfers, and that (ii) their calculated rates did not diverge at low densities (see Fig. 1).

A serious drawback of Bhattacharyya and Singwi's approach is that the calculated rates for $r_s > 4$ depend strongly on an undetermined parameter a_{21} . They adjust the value of a_{21} until the calculated rate at $r_s = 6$ agrees with the experimental rate. Since the additional term, which is proportional to a_{21} , contributes appreciably only in the region $r_s > 4$, it is clear from inspection of Fig. 1 that they are practically guaranteed a good

fit over the experimental range $2 \leq r_s \leq 6$ if they choose this value for a_{21} . Until a_{21} can be independently determined their theory is strongly parameter dependent. Moreover, with this value of a_{21} the calculated rate in this theory does not have the correct low-density-limiting behavior. For $r_s \geq 7$ the rate drops toward zero,²² instead of asymptotically approaching the spin-averaged positronium rate of 2.01 nsec^{-1} .

II. POSITRON-ELECTRON EFFECTIVE INTERACTION

To calculate the positron-annihilation rate, we need the positron-electron correlation function at zero separation $g_{+-}(\mathbf{r}=0)$. This problem is more complicated than the calculation in LB of the electron-electron correlation function $g(\mathbf{r}=0)$ for the pure-electron gas, but we find certain analogies with that problem help to make the present problem tractable.

A. Effective interaction at small separations

In order to determine $g_{+-}(\mathbf{r}=0)$ we must first construct the effective positron-electron interaction for small separations. In this section we restrict ourselves to momentum transfers greater than the Fermi momentum k_F . We associate momentum transfers smaller than k_F with the overall polarization of the medium, and we consider this effect in Sec. II B.

In the present section we argue that for momentum transfers greater than k_F , the dominant contributions to the effective interaction come from terms with no more than one screening electron excited at any instant. There are two main causes for this. First, if two electrons and a positron are close to each other they will strongly repel any additional electrons which approach them. Second, when three or more electrons are close to a positron Fermi statistics will necessarily play an important role. We would grossly overestimate the total contribution of such terms if we included only their direct parts. Since it is impractical to calculate the exchange parts, we prefer to omit the direct parts which themselves are already small.

We conclude the section by showing that if we consider only the dominant terms with a single excited screening electron at any instant, then the infinite summation of the screened interactions reduces to a tractable ladder sum. This is an important property since it is not generally true for retarded interactions.

Our arguments are similar to those in LB. In this problem, however, when a positron and an electron are close together it costs very little energy for a second electron to approach them

since the positron-electron pair has no net charge. By the uncertainty principle this electron can remain close to the pair for a long time. However, any further electrons will be repelled by this three-particle entity, so that a third electron can only approach at considerable energy cost. Thus, the uncertainty principle does not restrict one electron from contributing to a strong retarded screening effect, but it does restrict more than one electron from contributing. In other words, most retardation effects of the screening should, at any particular instant, be caused by one and only one screening electron. Exchange effects reinforce this conclusion. Whereas a positron and two antiparallel spin electrons can come close together without any cancellations from exchange, when a positron and three electrons are close there will always be exchange terms. These exchange terms will tend to cancel with the direct terms.

We see explicit cancellations of certain low-order direct and exchange diagrams when two screening electrons are in excited states at the same instant in time. Consider Fig. 2 for $p > k_F$. If the screening electron and the scattered electron have parallel spin, there is a leading-order cancellation between the direct and exchange diagram. If the two electrons have antiparallel spins there is no exchange term, so this spin configuration gives a contribution $O(p/k_F)$ larger than the configuration with parallel spins.

Let us therefore restrict the scattered and screening electrons to have antiparallel spin. In this case there is a leading order cancellation of direct and exchange diagrams when the excitations of two screening electrons overlap in time. Comparing Figs. 3(a) and 4(a), we see that their main difference is that in Fig. 3(a) the two excited screening electrons overlap in time, while in Fig. 4(a) the screening electrons do not overlap.

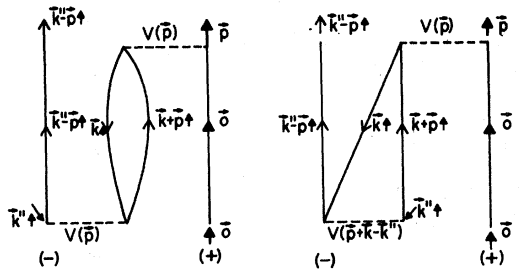


FIG. 2. There is a leading order cancellation of the direct and exchange diagram when the screening electron has spin parallel to the scattered electron. Open arrows indicate electrons; shaded arrows the positron.

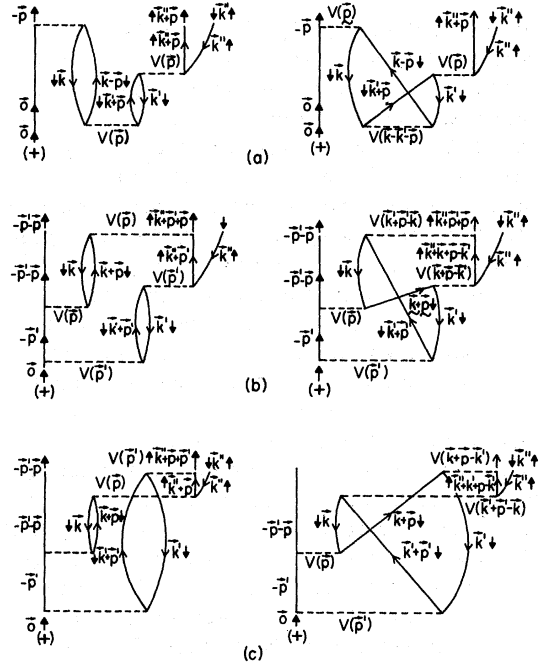


FIG. 3. For screening electrons with spin antiparallel to the scattered electron, there is leading-order cancellation of direct and exchange terms whenever two excited screening electrons overlap in time.

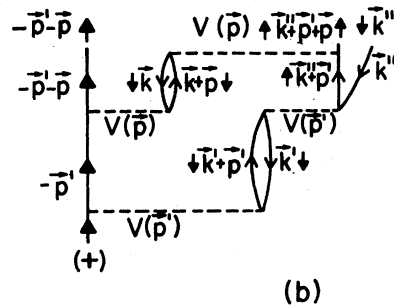
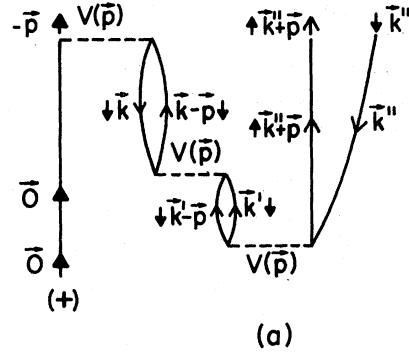


FIG. 4. For screening electrons with spin antiparallel to the scattered electron and with no overlaps in time, there are no exchange diagrams and hence no exchange cancellations.

Because of this, Fig. 3(a) has an exchange diagram which cancels the direct diagram to leading order in k_F/p , so that the sum of Figs. 3(a) are $O(k_F/p)$ smaller than Fig. 4(a). Similar arguments show that the sum of Figs. 3(b) are $O(k_F/p)$ smaller than Fig. 4(b), and that Fig. 3(c) has an exchange diagram which cancels its direct diagram to leading order in k_F/p . Note that Fig. 3(c) shows the retarded interactions cannot cross over in time without exchange cancellations reducing their contribution. These are three examples of how statistics cooperate with the repulsive electron-electron interaction to reduce contributions from terms where more than one screening electron is excited at any one instant.

The dominant terms with only one screening electron can be summed iteratively, in spite of the fact that the screened interaction is explicitly retarded. The retarded interactions can be time ordered, since the polarization bubbles cannot overlap in time. Since the interactions do not overlap and since only Tamm Dancoff (TDA) terms²³ are retained (Fig. 5), each interaction remains a constant and well-defined distance off the energy shell.

Our arguments do not eliminate the class of diagrams where one unscreened interaction overlaps a single retarded interaction (Fig. 6) and in order to make the calculation tractable we must rather arbitrarily neglect these terms. We defer consideration of self-energy insertions until Sec. II D, and correlations of the screening electrons until Sec. II E.

We now show that the sum of all the diagrams we have retained are included in the solution of a Lippmann-Schwinger integral equation,

$$\begin{aligned} \langle \vec{p} \vec{K} | t_{ep}(E = \epsilon_+ + \epsilon_-) | \vec{k}_0 \vec{K} \rangle &= \langle \vec{p} \vec{K} | V_{\text{eff}}(E) | \vec{k}_0 \vec{K} \rangle \\ &+ \int \frac{d^3q}{(2\pi)^3} \langle \vec{p} \vec{K} | V_{\text{eff}}(E) | \vec{q} \vec{K} \rangle \\ &\times [1/(E - q^2 - \frac{1}{4}K^2)] \langle \vec{q} \vec{K} | t_{ep}(E) | \vec{k}_0 \vec{K} \rangle, \end{aligned} \tag{3}$$

where $V_{\text{eff}}(E)$ is a screened retarded interaction which we shall define presently, $|\vec{p} \vec{K}\rangle$ is a positron-electron plane-wave state with relative momentum \vec{p} and center-of-mass momentum \vec{K} , $|\vec{k}_0 \vec{K}\rangle$ is the initial positron-electron state, and ϵ_{\pm} are the initial energies of positron and electron. The scattered electron is not antisymmetrized with the other electrons in the electron gas. We discuss in Sec. III how to carry out the antisymmetrization. A typical term in the sum of diagrams we have retained is shown in Fig. 5.

If we integrate over the time variables in Fig. 5

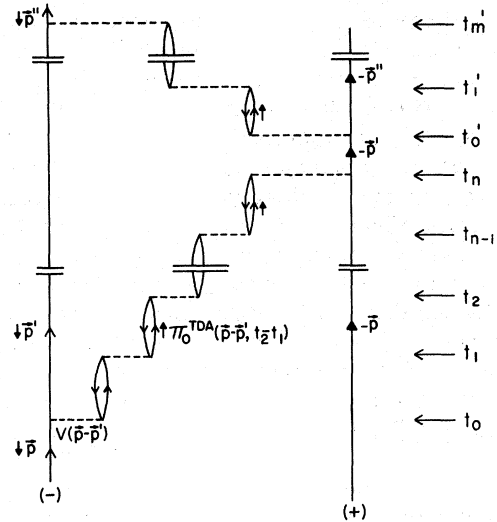


FIG. 5. Typical contribution to screened interactions when no more than one screening electron is excited at any instant. Note (i) we can time order these interactions, and (ii) each screening electron is excited a well-defined distance off the energy shell.

with the restrictions

$$t_0 \leq t_1 \leq \dots \leq t_{n-1} \leq t_n \leq t_0' \leq t_1' \leq \dots \leq t_m' \tag{4}$$

and then sum over the number of polarization bubbles m and n , we get

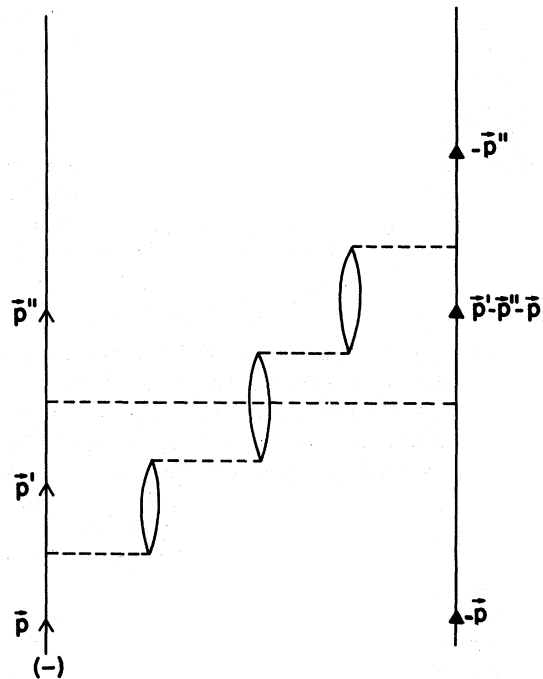


FIG. 6. One screened and one unscreened interaction can overlap in time without restrictions. We must neglect these terms.

$$\frac{V(|\vec{q}'|)}{1 - \Pi_0^{\text{TDA}}(\vec{q}', E')V(|\vec{q}'|)} \frac{1}{p'^2 - \epsilon_+ - \epsilon_- - i\eta} \frac{V(|\vec{q}''|)}{1 - \Pi_0^{\text{TDA}}(\vec{q}'', E'')V(|\vec{q}''|)}, \quad (5)$$

$$E' = \frac{1}{2}p'^2 + \frac{1}{2}p^2 - \epsilon_+ - \epsilon_-, \quad E'' = \frac{1}{2}p''^2 + \frac{1}{2}p^2 - \epsilon_+ - \epsilon_-,$$

$$\vec{q}' \equiv \vec{p}' - \vec{p}, \quad \vec{q}'' \equiv \vec{p}'' - \vec{p}',$$

and Π_0^{TDA} is the forward-time part of the Lindhard function Π_0 without the sum over spins,

$$\Pi_0^{\text{TDA}}(\vec{p}, t) = \begin{cases} (-1) \int_{|\vec{k}| < k_F}^{|\vec{p} + \vec{k}| > k_F} [d^3k / (2\pi)^3] e^{-i(\vec{p} + \vec{k})^2 t / 2} e^{-\eta t}, & t \geq 0 \\ 0, & t < 0 \end{cases} \quad (6)$$

$$\Pi_0^{\text{TDA}}(\vec{p}, E) = (i/\hbar) \int_0^\infty dt e^{iEt} \Pi_0^{\text{TDA}}(\vec{p}, t).$$

Each of the interactions in Fig. 5, with the exception of the unscreened term, can also have the opposite time flow direction. Adding these terms we get

$$\langle \vec{p} | V_{\text{eff}}(E) | \vec{p}' \rangle \frac{1}{p'^2 - \epsilon_+ - \epsilon_- - i\eta} \times \langle \vec{p}' | V_{\text{eff}}(E) | \vec{p}'' \rangle, \quad (7)$$

where

$$\langle \vec{p} | V_{\text{eff}}(E) | \vec{p}' \rangle = V(|\vec{p} - \vec{p}'|) + \frac{2\Pi_0^{\text{TDA}}(|\vec{p} - \vec{p}'|, E')V(|\vec{p} - \vec{p}'|)}{1 - \Pi_0^{\text{TDA}}(|\vec{p} - \vec{p}'|, E')V(|\vec{p} - \vec{p}'|)} \quad (8)$$

$$E' = \frac{1}{2}p^2 + \frac{1}{2}p'^2 - E.$$

Equation (7) shows clearly that the contribution to Fig. 5 is part of a Lippmann-Schwinger iterative sum for the effective interaction $V_{\text{eff}}(E)$ defined by Eq. (8).

B. Long-wavelength screening

We now consider the nature of the effective interaction for small momentum transfers. In this region exchange diagrams are negligible. Since the wavelengths of the screening excitations are greater than the average electron spacing, it is apparent that any screening must be a truly collective effect involving many electrons simultaneously. In LB we argue that for the pure electron gas the long-wavelength collective screening effects should be small for a pair of close electrons, since the pair will polarize the surrounding medium symmetrically. However, a positron and an electron have opposite charges, and even when they are close together, they will polarize the surrounding electron medium asymmetrically.

The polarization will have a dipolar pattern which will reduce the effective charge of both the positron and the electron. We would thus expect long-wavelength screening to be important. However, the instantaneous pair-correlation function for small separations should not be too sensitive to the details of this over-all polarization, and a Thomas-Fermi-type approximation²³ for this screening should be sufficient. Thus, for very small momentum transfers the effective interaction should be simply the static random-phase approximation (RPA) interaction,

$$\langle \vec{p} | V_{\text{eff}}(E) | \vec{p}' \rangle_{|\vec{p} - \vec{p}'| < k_F} = \frac{V(|\vec{p} - \vec{p}'|)}{1 - \Pi_0(|\vec{p} - \vec{p}'|, 0)V(|\vec{p} - \vec{p}'|)}. \quad (9)$$

Here $\Pi_0(p, 0)$ is the static Lindhard function which includes the sum over spins. We would expect a smooth transition from the TDA effective interaction of Eq. (8) to the RPA effective interaction of Eq. (9) for momentum transfers on the order of k_F . Our calculations have been performed using a discontinuous transition from Eq. (8) to Eq. (9) at a momentum transfer of k_F . A linear interpolation between the TDA and RPA effective interactions in the momentum-transfer region of k_F to $2k_F$ resulted in $\sim 2\%$ changes in positron-annihilation rates and indicates that the details of the transition are not of importance for the present problem.

C. Construction of electron-positron wave functions

The wave function for a given electron-positron pair may be obtained from the solution of the half-shell Lippmann-Schwinger equation (3) using the electron-positron effective interaction defined by

Eqs. (8) and (9). Since $V_{\text{eff}}(E)$ and, hence, $t_{\text{ep}}^K(E)$, depends only on the magnitude of the center of mass momentum, it is convenient to consider the partial wave decomposition of Eq. (3):

$$\langle p | t_i(E) | k_0 \rangle = \langle p | V_i(E) | k_0 \rangle + (2/\pi) \int q^2 dq \langle p | V_i(E) | q \rangle \times \frac{1}{E - q^2 - \frac{1}{4}K^2 + i\eta} \langle q | t_i(E) | k_0 \rangle. \quad (10)$$

Here,

$$\langle p | V_i(E) | k_0 \rangle = (1/8\pi) \int_{-1}^1 dz P_i(z) \langle \vec{p} | V_{\text{eff}}(E) | \vec{k}_0 \rangle, \quad (11)$$

where z is the cosine of the angle between \vec{p} and \vec{k}_0 . As noted above, E represents the energy of the initial electron-positron state. For numerical purposes it is convenient to employ standing-wave boundary conditions so that all quantities appearing in Eq. (10) are real. [This means only that the integral on the right-hand side of Eq. (10) is treated as a principal-value integral.] The equation may be cast in a manifestly Fredholm form using the transformation of Kowalski²⁴ and can thus be solved numerically by replacing the integral by a weighted sum over a suitably chosen mesh of points. The solution may be converted to outgoing boundary conditions through an appropriate change of normalization.

The electron-positron wave function is related to the half-shell t matrix by

$$\langle \vec{p} | V_{\text{eff}}(E) | \psi^{\vec{k}, \vec{k}_0} \rangle = \langle \vec{p} | t^K(E) | \vec{k}_0 \rangle. \quad (12)$$

Alternatively, we may use the Schrödinger equation to write

$$\langle \vec{p} | \psi^{\vec{k}, \vec{k}_0} \rangle = [1/(E - p^2)] \langle \vec{p} | t^K(E) | \vec{k}_0 \rangle. \quad (13)$$

The electron-positron wave function in coordinate space, $\psi^{\vec{k}, \vec{k}_0}(r)$, is obtained as the Fourier transform of Eq. (13). The pair-correlation function for the initial state $|\vec{k}, \vec{k}_0\rangle$ may finally be obtained as

$$g_{+-}^{\vec{k}, \vec{k}_0}(r) = |\psi^{\vec{k}, \vec{k}_0}(r)|^2.$$

Since the present problem involves only the correlation function at $r=0$, we need solve the Lippmann-Schwinger equation only for the $l=0$ partial wave. The formidable problems of constructing Fourier transforms numerically are also absent in the special case $r=0$ where it is adequate to use the same mesh of points employed in the solution of the Lippmann-Schwinger equation.

D. Self-energy insertions

We have argued that one screening electron could strongly screen the positron-electron interaction. This one electron could equally well interact strongly with only the positron or only the electron, to give significant self-energy contributions. Using our arguments about leading order cancellations of direct and exchange diagrams, we may exclude vertex corrections such as Figs. 7(a) or 7(b). For self-energy insertions on the intermediate propagators between interactions, such as Fig. 7(c), there are no such cancellations, and we approximate their effect by adding RPA self-energies to the single-particle energies (see the Appendix),

$$\epsilon_{\pm}(\vec{q}) = \frac{1}{2} |\vec{q}|^2 + \Sigma_{\text{RPA}}^{(e,p)}(\vec{q}, \epsilon_{\mp}). \quad (14)$$

These energies are used in the Lippmann-Sch-

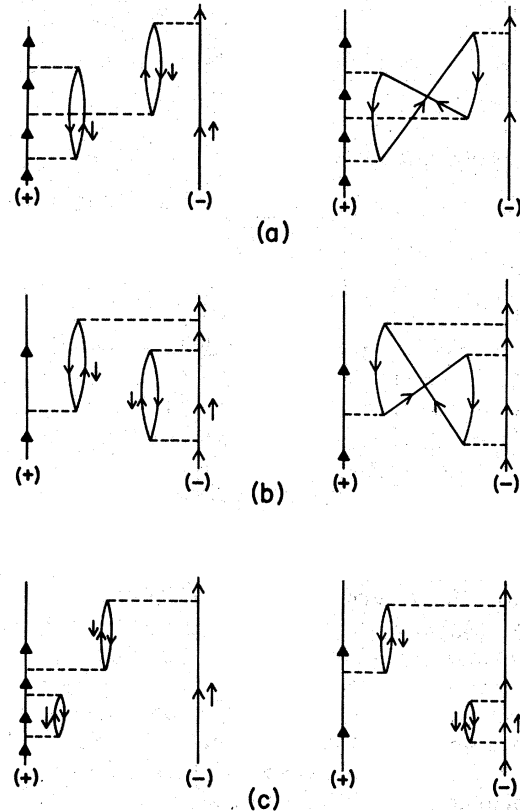


FIG. 7. Vertex corrections (a) and (b) show leading order cancellations of direct and exchange diagrams. Self-energy insertions (c) on the intermediate propagator lines do not have exchange diagrams unless they overlap in time with a screened interaction.

winger Eq. (3). Since

$$\Sigma_{\text{RPA}}^{(e,p)}(\frac{1}{2}\vec{K} \pm \vec{q}, \epsilon_{\pm}(\frac{1}{2}\vec{K} \pm \vec{q}))$$

are slowly varying functions of \vec{K} for $0 \leq |\frac{1}{2}\vec{K}| \leq k_F$, we averaged both functions over the angle \vec{K} to obtain $t_{\text{ep}}^K(E)$ as a function only of $|\vec{K}|$. The remainder of the calculation for $\langle \vec{p}\vec{K} | t_{\text{ep}}^K(E) | \vec{k}_0\vec{K} \rangle$ can then be performed without further modification. These insertions reduced the wave functions at the origin by about 5% and the annihilation rates by 10%.

E. Correlations of screening electrons

Kahana⁷ has shown that the observed buildup of electron density around a positron could only be accounted for by summing the positron-electron effective interaction to infinite order. The importance of screening the effective interaction is also well known. In previous sections we have considered the effect of screening excitations only within the linear-response RPA theory. To be consistent we must take into account the nonlinear buildup of screening charge around the positron. Otherwise we shall underestimate the effect of screening.

In this section we approximately include corre-

lations of the screening electron by replacing each bare Coulomb interaction in our expression for $V_{\text{eff}}(E)$ with the appropriate ladder sum of interactions. Each electron-electron interaction is replaced by either the ladder sum of unscreened Coulomb interactions t_{ee} or its local approximation t_{ee}^{loc} , both of which are defined and calculated in LB. The positron-screening electron interaction is replaced by t_{ep} as calculated in the previous sections for the uncorrelated screening electron. This procedure is analogous with our construction of t_{eff} in LB.

We have approximately treated correlations between a screening electron and the positron (t_{ep}), correlations between two screening electrons (t_{ee}^{loc}), and correlations between a screening electron and the scattered electron (t_{ee}). Because the initial state for the scattered electron-screening electron interaction is not generally within the Fermi sea, we must use t_{ee} rather than t_{ee}^{loc} for this particular interaction. For momentum transfers $|\vec{q}| > k_F$, each interaction is a well-defined distance off the energy shell; for $|\vec{q}| < k_F$ we use the static approximation for the off-shell effects. Thus the effective positron-electron interaction with correlated screening electrons $V_{\text{eff}}^{(1)}$ is defined as (Fig. 8)

$$\begin{aligned} \langle \vec{q}\vec{K} | V_{\text{eff}}^{(1)}(E) | \vec{k}\vec{K} \rangle = & V(|\vec{q} - \vec{k}|) + \left(\frac{1}{\frac{4}{3}\pi k_F^3} \int_{|\vec{p}''| < k_F} d^3p'' \langle \frac{1}{2}(\frac{1}{2}\vec{K} + \vec{q} - \vec{p}'') | t_{ee}^{(\vec{K} + \vec{q} + \vec{p}'')/2}(E_e) | \frac{1}{2}(\frac{1}{2}\vec{K} + 2\vec{k} - \vec{q} - \vec{p}'') \rangle \right. \\ & \times [f(|\vec{q} - \vec{k}|, \omega)] \frac{1}{\frac{4}{3}\pi k_F^3} \int_{|\vec{p}| < k_F} d^3p \langle \frac{1}{2}(\vec{p} + 2\vec{q} - \vec{k} - \frac{1}{2}\vec{K}) | t_{\text{ep}}^{(\vec{K} - \vec{k} - \vec{p})/2}(E_p) | \frac{1}{2}(-\frac{1}{2}\vec{K} + \vec{p} + \vec{k}) \rangle \\ & \left. + (\vec{q} \leftrightarrow \vec{k}) \right), \end{aligned} \quad (15)$$

where for $|\vec{q} - \vec{k}| \geq k_F$

$$f(|q - k|, \omega) = \frac{2\Pi_0^{\text{TDA}}(|\vec{q} - \vec{k}|, \omega)}{1 - t_{ee}^{\text{loc}}(|\vec{q} - \vec{k}|)\Pi_0^{\text{TDA}}(|\vec{q} - \vec{k}|, \omega)}, \quad (16)$$

$$E_e = E + \frac{1}{2}p''^2 - \frac{1}{2}(\frac{1}{2}\vec{K} - \vec{q})^2, \quad E_p = E + \frac{1}{2}p^2 - \frac{1}{2}(\frac{1}{2}\vec{K} + \vec{k})^2, \quad \omega = \frac{1}{2}(\frac{1}{2}\vec{K} - \vec{q})^2 + \frac{1}{2}(\frac{1}{2}\vec{K} + \vec{k})^2 - E;$$

while for $|\vec{q} - \vec{k}| < k_F$

$$f(|\vec{q} - \vec{k}|, \omega) = \frac{2\Pi_0(|\vec{q} - \vec{k}|, 0)}{1 - t_{ee}^{\text{loc}}(|\vec{q} - \vec{k}|)\Pi_0(|\vec{q} - \vec{k}|, 0)}, \quad (17)$$

$$E_e = \frac{1}{2}p''^2, \quad E_p = \frac{1}{2}p^2, \quad \omega = 0.$$

Because of the rather long computing time, we had to average each momentum vector in the expression for $V_{\text{eff}}^{(1)}$ over the directions \hat{p}'' , \hat{p} , and \hat{K} . If screening-electron correlations are unimportant, V_{eff} and $V_{\text{eff}}^{(1)}$ become identical since we

may recover V_{eff} from $V_{\text{eff}}^{(1)}$ simply by replacing t_{ee} , t_{ee}^{loc} , and t_{ep} by V_{ee} and V_{ep} . Using the Low equation²⁵ to efficiently compute the off-energy-shell values of $t_{\text{ep}}(E)$ and $t_{ee}(E)$, we could calculate $V_{\text{eff}}^{(1)}$ numerically.

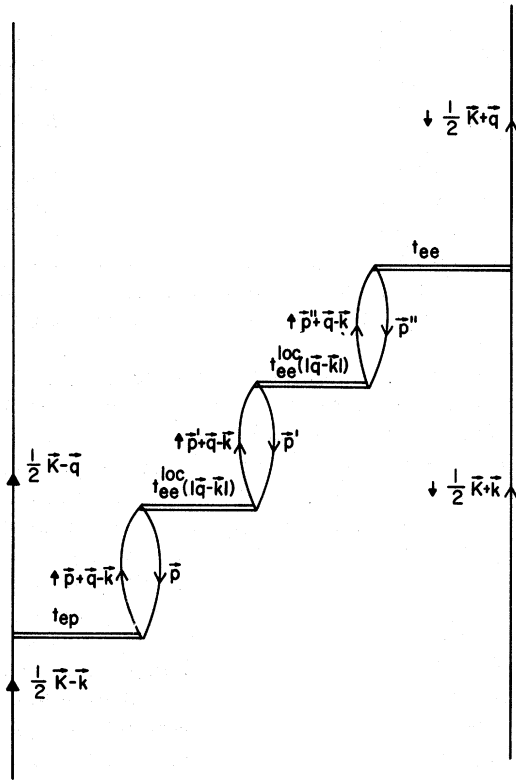


FIG. 8. Typical contribution to $V_{\text{eff}}^{(1)}$, the effective positron-electron interaction with correlated screening electrons. Here t_{ep} is the ladder sum of effective positron-electron interactions with uncorrelated screening electrons V_{eff} , t_{ee} is the ladder sum of unscreened electron-electron Coulomb interactions, and $t_{\text{ee}}^{\text{loc}}(|\vec{q}-\vec{k}|)$ is a local approximation to t_{ee} , both calculated in Ref. 1. The equivalent contribution for V_{eff} would be with t_{ep} , t_{ee} , and $t_{\text{ee}}^{\text{loc}}$ all replaced by Coulomb interactions.

Replacement of V_{ee} by t_{ee} tends to reduce the density of screening electrons between the positron and electron while the replacement of V_{ep} by t_{ep} tends to increase the density of screening electrons. The latter effect is dominant so that $V_{\text{eff}}^{(1)}$ is markedly less attractive than V_{eff} for small and intermediate momentum transfers. The replacement of V_{eff} by $V_{\text{eff}}^{(1)}$ in Eq. (3) leads to a reduction of the positron-electron wave functions for zero separation of approximately 30%. The new wave functions also show considerably less variation across the Fermi sea of initial electron states. The magnitude of the reduction of $g_{+-}(r=0)$ confirms the importance of screening-electron correlations in the calculation of positron-annihilation rates.

This procedure could have been repeated to obtain $V_{\text{eff}}^{(2)}$ by replacing the t_{ep} in Eq. (15) by the $t_{\text{ep}}^{(1)}$ obtained using $V_{\text{eff}}^{(1)}$ in Eq. (3). This iteration pro-

cess could be repeated until self-consistent values of t_{ep} (and, hence, self-consistent electron-positron wave functions) were obtained. However, consideration of the diagrams added in each iteration indicates that an unlimited number of screening electrons could contribute to the final self-consistent V_{eff} . Since our previous arguments suggest that there should be extensive cancellations with exchange diagrams not included in such an iterative procedure, additional iterations are expected to overestimate the correction to the wave function. Thus, we have approximated all positron-screening electron correlations by the use of $V_{\text{eff}}^{(1)}$ defined by Eq. (15). In fact, the additional corrections to the wave function from higher iterations were found to be only on the order of 4%. This suggests that the use of Eq. (15) is probably quite reliable.

III. ANTISYMMETRIZATION OF ELECTRON WAVE FUNCTIONS

In Sec. II we calculated the correlation of a particular unsymmetrized electron by the positron, using the two-body Lippmann-Schwinger integral equation with a complicated effective interaction. We now turn to the problem of how to antisymmetrize this particular electron with all the other electrons.

A. Bethe-Goldstone equation

We first examine the Bethe-Goldstone equation which, as we have mentioned, has previously been used to antisymmetrize the electron wave functions in the calculation of both short-range electron-electron correlations^{1,26} and short-range positron-electron correlations.⁷ We find that the Bethe-Goldstone equation correctly antisymmetrizes the electron wave functions for electron-electron correlations. In contrast, however, we shall find in Sec. III B that for the positron-electron correlation function, the Bethe-Goldstone equation does not correctly antisymmetrize the electron wave functions. In Sec. IV B we are able to show that the divergence in the Bethe-Goldstone rates at low density (Fig. 1) is directly attributable to this misuse of the Bethe-Goldstone equation.

In LB the Bethe-Goldstone was used to calculate the antisymmetrized electron-electron wave function at short distances. Let us examine how the Bethe-Goldstone equation correctly antisymmetrized this wave function. For two labeled unsymmetrized electrons i and j , the two-body interacting wave function ψ_{ij} is given by the Lippmann-Schwinger equation. For the pure-electron gas, we argued that only the electrons i and j them-

selves are perturbed, so the antisymmetrized N -body ground-state wave function is

$$\Psi_N^A = A(\Phi_1^{(1)}\Phi_2^{(2)}\dots\psi_{ij}^{(ij)}\dots\Phi_N^{(N)}), \quad (18)$$

where A is the antisymmetry operator,

$$\Phi_k^{(k)} \equiv \Phi^{(k)}(\vec{p}_k),$$

$$\Psi_N^A = A \left[\left(\Phi_i^{(i)} \Phi_j^{(j)} + \int \frac{d^3 p'}{(2\pi)^3} \Phi_i^{(i)} \Phi_{j'}^{(j)} \frac{Q(\vec{p}_i, \vec{p}_{j'}, k_F)}{p^2 - p'^2} \langle \Phi_i^{(i)} \Phi_{j'}^{(j)} | V | \psi_{ij}^{(ij)} \rangle \right) \prod_{\substack{k=1, \\ k \neq i, j}}^N \Phi_k^{(k)} \right] \quad (19)$$

$$= A \left(\psi_{ij}^{\text{BG}} \prod_{\substack{k=1, \\ k \neq i, j}}^N \Phi_k^{(k)} \right), \quad (20)$$

where Q is the Pauli projection operator,

$$Q(\vec{p}_i, \vec{p}_j, k_F) = \Theta(|\vec{p}_i| - k_F) \Theta(|\vec{p}_j| - k_F), \quad (21)$$

$$\vec{p} = \vec{p}_i - \vec{p}_j, \quad \vec{p}' = \vec{p}_i' - \vec{p}_j', \quad \vec{p}_i + \vec{p}_j = \vec{p}_i' + \vec{p}_j', \quad (22)$$

and ψ_{ij}^{BG} is the two-body Bethe-Goldstone wave function. Thus, if only the two scattered electrons are perturbed, use of the Bethe-Goldstone equation leads to a correctly antisymmetrized wave function.

It is straightforward to show that the Lippmann-Schwinger wave functions are mutually orthogonal and that the Bethe-Goldstone wave-functions are not:

$$\langle \psi_{km}^{\text{BG}} | \psi_{ij}^{\text{BG}} \rangle \neq 0. \quad (23)$$

Due to the Pauli operator, the Bethe-Goldstone wave functions are orthogonal to the unperturbed states below the Fermi sea,

$$\langle \Phi_k \Phi_m | \psi_{ij}^{\text{BG}} \rangle = 0 \text{ if } p_k, p_m < k_F \text{ and } (km) \neq (ij). \quad (24)$$

Thus, if the other $N-2$ wave functions are unexcited by the scattering, the N -body ground-state wave function

$$\Psi_N^A = A \left(\psi_{ij}^{\text{BG}} \prod_{\substack{k=1, \\ k \neq i, j}}^N \Phi_k^{(k)} \right) \quad (25)$$

is still a Slater determinant of N mutually orthogonal single-particle wave functions. It follows that the expectation value of any two-body operator O_2 will reduce to

$$\langle \Psi_N^A | O_2 | \Psi_N^A \rangle = \sum_{i < j}^N \langle \psi_{ij}^{\text{BG}} | O_2 | \psi_{ij}^{\text{BG}} \rangle. \quad (26)$$

The electron-electron correlation function $g(r)$ is the expectation value of the density operator squared, which is a two-body operator. Thus

and all starting momenta are less than k_F .

Using the Lippmann-Schwinger equation (LSE) to define ψ_{ij} in terms of unperturbed states and performing some of the interchanges implied by A , it immediately follows that

$g(r)$ is given by

$$g(r) = \sum_{p_i, p_j < k_F} |\langle \psi_{ij}^{\text{BG}} | \vec{r} \rangle|^2. \quad (27)$$

We conclude that if the two scattered electrons are the only particles perturbed, the Bethe-Goldstone formalism correctly calculates the pair correlation-function for the antisymmetrized N -electron ground state.

B. Inhomogeneous electron gas

Returning to the positron problem, we note that the positron is an impurity which destroys the homogeneity of the electron gas. Since the electrons will scatter off the impurity, the Hartree-Fock solutions to the inhomogeneous problem will differ from the Hartree-Fock solutions for the pure-electron gas. Thus even at distances from the impurity so large that the impurity potential has been completely screened out, the exact single-electron wave functions for the inhomogeneous system will be phase shifted away from the unperturbed plane-wave states. The impurity perturbs all the electrons from their plane-wave states, so that the Bethe-Goldstone equation (BGE) employed by Kahana⁷ is inappropriate for this problem since it uses the unperturbed plane-wave basis. In particular, the plane-wave BGE requires that the momentum threshold for scattering be greater than zero, and this is not true when the system includes an impurity. It is of course difficult to start from other than a plane-wave basis for a finite-mass impurity, making it impractical to apply the BGE to this problem.

We now show that if we could neglect the recoil of the positron it would be quite straightforward to calculate $g_{+-}(r)$ from the solutions of the Lippmann-Schwinger equations. We could probably neglect the positron recoil should it become

trapped, for example, at a crystal defect. Such trapping is frequently observed in aluminum, but not in the alkali metals.²

We have included in our effective impurity potential $V_{\text{eff}}^{(1)}$ only screening effects caused by excited electrons with spin antiparallel to that of the electron being scattered by $V_{\text{eff}}^{(1)}$. Arbitrarily assigning spin up to this electron, we are thus excluding all terms in which there are excited spin-up screening electrons, arguing that the total contribution of such terms after antisymmetrization is small. Hence, within our model, antisymmetrization of the spin-up electrons is not affected by excitations of screening electrons since the latter all have spin down and are thus a distinguishable species. Calculating the electron correlation function $g_{+-}(r)$ for this system is straightforward since the spin-up electrons form a one-component system of noninteracting fermions moving in the external potential $V_{\text{eff}}^{(1)}$. With the positron fixed at the origin and omitting the spin-up labels, $g_{+-}(r)$ for spin-up electrons is given by

$$g_{+-}(r_1) = \int dr_2 \cdots dr_N \{A[\psi^{(1)}(\vec{r}_1) \cdots \psi^{(i)}(\vec{r}_i) \cdots \psi^{N/2}(\vec{r}_{N/2})]\} \times \{A[\psi^{(1)}(\vec{r}_1) \cdots \psi^{(j)}(\vec{r}_j) \cdots \psi^{N/2}(\vec{r}_{N/2})]\}^* \quad (28)$$

Here $\psi^{(j)}(\vec{r})$ is the normalized solution of the one-body Lippmann-Schwinger equation for the spin-up electron (j),

$$\psi^{(j)}(\vec{r}) = \int \frac{d^3k}{(2\pi)^3} e^{i\vec{k} \cdot \vec{r}} \psi_k^{(j)},$$

$$\psi_k^{(j)} = \Phi_k^{(j)} + \int \frac{d^3k'}{(2\pi)^3} \Phi_k^{(j)} \frac{1}{k^2 - k'^2} \times \langle \Phi_k^{(j)} | V_{\text{eff}}^{(1)} | \psi_k^{(j)} \rangle, \quad (29)$$

where $\frac{1}{2}k^2 = E_k$ and $\frac{1}{2}k'^2 = E_{k'}$ and

$$0 = E_1 < E_2 < \cdots < E_{N/2} = \frac{1}{2}k_F^2. \quad (30)$$

Since the $\psi_k^{(j)}$ form an orthonormal set, it follows that the positron-electron-correlation function for a spin-up electron is

$$g_{+-}(r_1) = \sum_{p_j < k_F} |\psi^{(j)}(r_1)|^2. \quad (31)$$

Writing the spin labels explicitly, the total contribution to $g_{+-}(r)$ from spin-up and spin-down electrons is

$$g_{+-}(r_1) = \sum_{\sigma=\pm} \sum_{p_j < k_F} |\psi_{\sigma}^{(j)}(r_1)|^2. \quad (32)$$

In Sec. III we solved the Lippmann-Schwinger equation, including positron recoil, and obtained the correlated positron-electron wave functions $|\psi_0^{\text{pos}} \psi_j^{(j)}\rangle$ as solutions. Including positron recoil, we can no longer calculate $g_{+-}(r)$ exactly, even within our model, since we do not know how to construct the many-body wave function from $|\psi_0^{\text{pos}} \psi_j^{(j)}\rangle$. Consequently, we simply follow the procedure that was correct in the recoilless case. Since the Lippmann-Schwinger wave functions $|\psi_0^{\text{pos}} \psi_j^{(j)}\rangle$ are mutually orthogonal, the pair-correlation function is then just the square of the two-body positron-electron wave functions,

$$g_{+-}(r) = \sum_{p_j < k_F} |\langle \psi_0^{\text{pos}} \psi_j^{(j)} | \vec{r} \rangle|^2, \quad (33)$$

where the antisymmetrization is automatically included when we average over the starting momentum $|\vec{p}_j| < k_F$. Since $g_{+-}(r=0)$ is the probability of finding an electron at the positron site, using Eq. (1) the annihilation rate is

$$R(r_s) = \frac{1}{4} \frac{R_{p_s}}{|\Phi_{p_s}(r=0)|^2} \frac{1}{\frac{4}{3}\pi(r_s a_0)^3} g_{+-}(r=0), \quad (34)$$

where a_0 is the Bohr radius. We discuss our calculated rates in Sec. V, but we first examine those modifications needed when the interaction permits the formation of bound states.

IV. BOUND STATES

When a positron and an electron interact in free space, their energy spectrum consists of a continuum of positive-energy scattering states and an infinite number of bound states. These latter states are bounded from below by the ¹S positronium ground state at energy -6.8 eV. When an electron is in this state it is localized in a spherically symmetric wave function around the positron so that it almost completely screens the positron's charge.

If we place the positron-electron ¹S bound state in a dilute electron-gas medium, the pair will polarize the medium, which will, in turn, screen the positron-electron interaction. This decreases the binding energy of the bound state, but our calculations indicate that the spatial bound-state wave function changes very little. The reason for this is that it is mainly the long-wave-length components of the wave function which are affected by screening, and these components are unimportant for a localized wave function. As we increase the density of the electron medium, and hence increase the screening, the bound-state wave function does not delocalize appreciably until its binding energy is almost zero. If

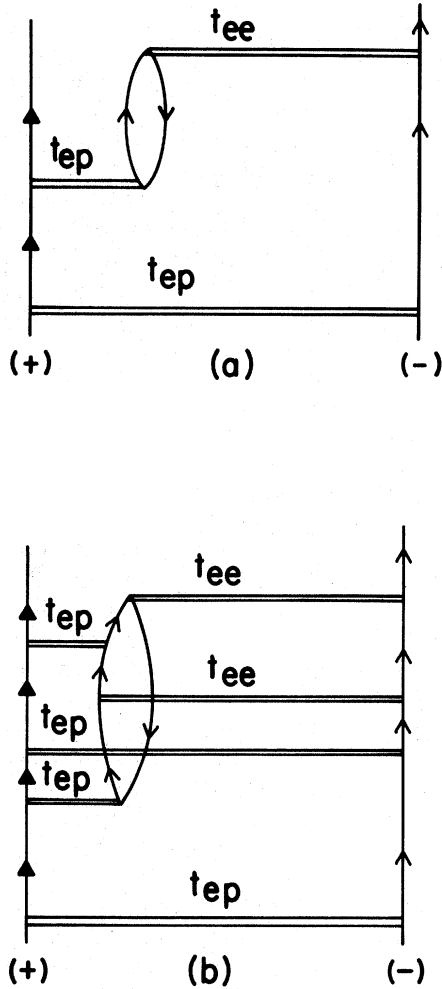


FIG. 9. When the screening electron is in a bound state for $r_s > 7$, it almost completely screens the positron charge. Terms of high order in t_{ep} and t_{ee} (b) contribute significantly to this effect.

we then increase the density only slightly, the state rapidly diffuses and merges with the continuum states at a density of $r_s = 6.2$. We note that this represents an electron density slightly lower than that found in Cs, the most dilute alkali metal. The Ps^- bound state behaves similarly but merges with the continuum at a much lower density. The density may be estimated in perturbation theory by replacing all Coulomb interactions with Yukawa potentials:

$$\Delta E = \langle \Phi_{\text{Ps}^-} | \sum_{i < j} e_i e_j \left(\frac{e^{-\mu r_{ij}} - 1}{r_{ij}} \right) | \Phi_{\text{Ps}^-} \rangle. \quad (35)$$

For the case of interest μ is sufficiently small to justify expansion of the exponential yielding $\Delta E = +e^2 \mu$. In the Thomas-Fermi approximation,

$$\mu^2 = (4/\pi a_0^2)(1/\alpha r_s), \quad (36)$$

where $a_0 \sim 0.52 \text{ \AA}$ is the Bohr radius and $\alpha = (4/9\pi)^{1/3}$. Setting $e^2 \mu$ equal to the Ps^- binding energy suggests that this bound state will not exist for $r_s < 3 \times 10^3$ and may thus be neglected for all metallic-electron densities.

For $6.2 < r_s < 3 \times 10^3$ the many-electron ground state will consist of a positron-electron ^1S bound state with the remaining electrons filling the lowest energy continuum states. Since the bound state remains localized, the positron will be very effectively screened by its bound electron and the continuum states will be only weakly perturbed from plane waves. In this situation the positron can annihilate with either the strongly correlated bound electron or the weakly correlated continuum electrons. The former process is expected to dominate.

A. Bound states for present calculation

In the present calculation, an electron-positron bound state will appear as a pole in the electron-positron t matrix, $t_{ep}(E)$ or $t_{ep}^{(1)}(E)$, at $E = -E_B$. The unnormalized bound-state wave function is easily recovered from the residue of this pole using Eqs. (12) and (13). In constructing $V_{\text{eff}}^{(1)}$ via Eq. (15), one may be led to integrate over a bound-state pole in $t_{ep}(E)$ corresponding to a bound state formed from the positron and a screening electron. From the above discussion of the Ps^- bound state it is clear that a bound screening electron, properly described, will screen the positron so thoroughly that no additional bound states will exist for normal metallic-electron densities. The inclusion of the effects of a bound screening electron is clearly appropriate for determining $V_{\text{eff}}^{(1)}$ for calculations of electron-continuum states (Fig. 9). For the calculation of electron bound states, $V_{\text{eff}}^{(1)}$ should include the screening effects of continuum electrons only. Thus, we have explicitly isolated and removed the pole in $t_{ep}(E)$ in the determination of $V_{\text{eff}}^{(1)}$ for the electron-positron bound state.

In Fig. 10(a) we show $-E_B^{1\text{S}}(r_s)$ for $t_{ep}^{(1)}$. In the zero-density limit $E_B^{1\text{S}}$ tends toward 6.8 eV, which is the binding energy of ^1S positronium in free space. As the density is increased, $E_B^{1\text{S}}$ smoothly decreases reaching zero at $r_s \approx 6.2$. Since the ^1S state is the positronium ground state, there can be no bound states at densities higher than $r_s \approx 6.2$. In Fig. 10(b) we show

$$\rho_{1\text{S}}(r=0) = |\psi_{1\text{S}}(r=0)|^2,$$

the bound-state electron density at the positron site. Since we normalize the wave function

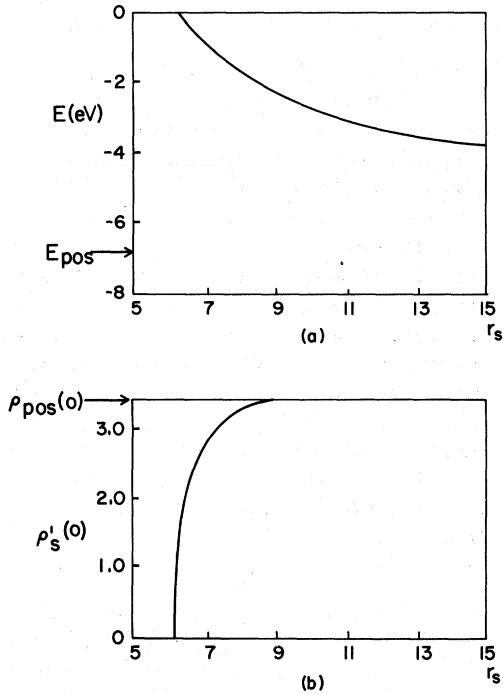


FIG. 10. (a) Position of $1S$ bound-state pole in $t_{ep}^{(1)}(E)$ as a function of r_s . This is equal to $-E_B^{1S}$, where E_B is the binding energy of the bound state. Note how slowly E_B^{1S} approaches 6.8 eV, the binding energy of $1S$ positronium in free space. (b) Electron density at positron site for $1S$ bound state $\rho_{1s}(r=0)$. The density for free-space positronium $\rho_{pos}(r=0)$ is 3.37 \AA^{-3} . Since the bound-state wave functions are normalized, $\rho_{1s}(0)$ also measures the degree of their localization. Note the wave functions remain localized until the binding energy is nearly zero.

$$\int d^3r |\psi_{1s}(\vec{r})|^2 = 1, \quad (37)$$

this is also a measure of the degree of localization of the wave function. The value of $\rho_{1s}(r=0)$ for free-space positronium is about 3.37 \AA^{-3} , and it remains constant at that value until the density is increased to $r_s \approx 7$. Between $r_s = 7$ and $r_s = 6.2$, as E_B goes to zero, $\rho_{1s}(r=0)$ drops rapidly to zero. Thus, although the binding energy is very sensitive to the amount of screening, the spatial wave function remains practically unchanged until the screening is so strong that the bound state ceases to exist. These properties are characteristic of a Yukawa-type potential.

Cesium has the lowest valence-electron density of the alkali metals at $r_s = 5.74$, and so our calculation predicts that screening is too strong for the positron to form bound states with electrons in any of the alkali metals. If positronium were to form in any of the metals, then, provided it

first thermalized, it should be detectable in the angular-distribution data of the emitted γ rays as a sharp spike at relative angle $\theta = \pi$. Unfortunately, it is difficult experimentally to reach the density region below $r_s = 5.74$. The alkali metals with low valence-electron densities, cesium and rubidium, both have low melting points, so their thermal expansion cannot be used to lower the density. If a positron were to get trapped near a negative-ion impurity in a cesium or rubidium lattice, it is possible that the average valence-electron density in the vicinity of the negative ion would be lowered sufficiently for positronium to be formed. A similar situation might occur if the positron were to get trapped on the surface of an alkali metal. It would be interesting to search for positronium under these experimental conditions.

When the bound state exists, its annihilation rate is proportional to $\rho_{1s}(r_s, r=0)$, and, referring again to Fig. 10(b), we see that the rate remains almost constant over the density range $7 < r_s < \infty$. It then drops rapidly to zero over the range $6.2 < r_s \leq 7$. We take the annihilation rate of spin-averaged positronium in free space as the proportionality constant which relates $\rho_{1s}(r_s, r=0)$ to the bound-state annihilation rate. In the absence of an external magnetic field, singlet $1S$ positronium and triplet $3S$ positronium are degenerate. In a metal, we would expect stray magnetic fields would be sufficient to maintain a statistical balance between the singlet and triplet states whenever either was depleted by annihilations. Singlet positronium annihilates with the emission of two γ rays with a rate of $8.0 \times 10^9 \text{ sec}^{-1}$. Because of angular-momentum conservation, triplet positronium must emit three γ rays when it annihilates and has the much lower rate of $7.1 \times 10^6 \text{ sec}^{-1}$. The spin-average of these rates is $2.0 \times 10^9 \text{ sec}^{-1}$; thus

$$R_{ps}(r_s) = \frac{\rho_{1s}(r_s, r=0)}{\rho_{1s}(r_s = \infty, r=0)} \times 2.0 \times 10^9 \text{ sec}^{-1}. \quad (38)$$

The contribution to the rate from the $1S$ positronium state for $r_s \geq 6.2$ is shown in Fig. 13.

We also estimated the contribution to the rate for $r_s \geq 7$, coming from annihilations with electrons in continuum states. We projected out screening-electron bound states from $V_{\text{eff}}^{(1)}$, since when the screening electron is in a $1S$ bound state for $r_s \geq 7$, it should so efficiently screen the positron's charge that the continuum electrons will remain practically unperturbed. Our calculated $V_{\text{eff}}^{(1)}$ did not show this effect since only terms of first order in t_{ep} and t_{ee} were included, Fig. 9(a). By setting $V_{\text{eff}}^{(1)} = 0$ when the screening electron is in such a bound state for $r_s \geq 7$, we are approxi-

mately including the additional screening coming from terms of higher order in t_{ep} and t_{ep} , Fig. 9(b). We show in Fig. 13 the contribution to the annihilation rates for $r_s \geq 7$ coming from the continuum states. As expected, the contribution to the rates from the bound state dominates for $r_s > 7$, and the continuum contribution decreases towards the noninteracting value.

B. Bound states for Bethe-Goldstone equation

We now examine the behavior of the bound-state poles if we inappropriately apply the Bethe-Goldstone equation discussed in Sec. IIIA to this problem. We find that the poles behave quite differently from the poles of the Lippmann-Schwinger equation. We show that the divergence in the annihilation rate at low density which occurred in previous diagrammatic calculations (see Sec. I and Fig. 1), is due to unphysical bound states generated by the Bethe-Goldstone equation. Qualitatively, our conclusions do not depend on the exact form of the effective interaction, so for simplicity we use the static RPA interaction,

$$V_{\text{RPA}}(\vec{q}) = V(\vec{q})/[1 - \Pi_0(\vec{q}, 0)V(\vec{q})], \quad (39)$$

which has been the interaction commonly used by previous authors.⁷

Let us examine the analytic structure of the Bethe-Goldstone effective interaction $t_{ep}^{\text{BG}}(E)$ on the real-energy axis. In free space, Fig. 11(a), t_{ep}^{BG} is identical to our previous solution. It has an infinite number of poles on the interval $-6.8 \text{ eV} \leq E < 0$, corresponding to the states of positronium, and it has a cut along the positive E axis with the branch point at $E = 0$. This cut corresponds to the positive energy-scattering states. At nonzero density for center-of-mass momentum $\vec{K} = 0$, $t_{ep}^{\text{BG}}(E)$ is a solution of the equation

$$t_{ep}^{\text{BG}}(E) = V_{\text{RPA}} + \int_{|\vec{q}| > k_F} \frac{d^3q}{(2\pi)^3} V_{\text{RPA}}(\vec{q}) \times \frac{1}{E - q^2} \langle \vec{q} | t_{ep}^{\text{BG}}(E) \rangle. \quad (40)$$

The analytic structure of $t_{ep}^{\text{BG}}(E)$ now differs fundamentally from the structure of $t_{ep}(E)$ which has no Pauli operator. The bound states of $t_{ep}^{\text{BG}}(E)$ have less binding energy than the corresponding states of $t_{ep}(E)$, because the Pauli operator projects out low-momentum components from the bound state. More importantly, the threshold for scattering solutions is at nonzero energy [Fig. 11(b)],

$$E_{\text{thresh}} = \epsilon_{\text{Fermi}} = k_F^2 > 0. \quad (41)$$

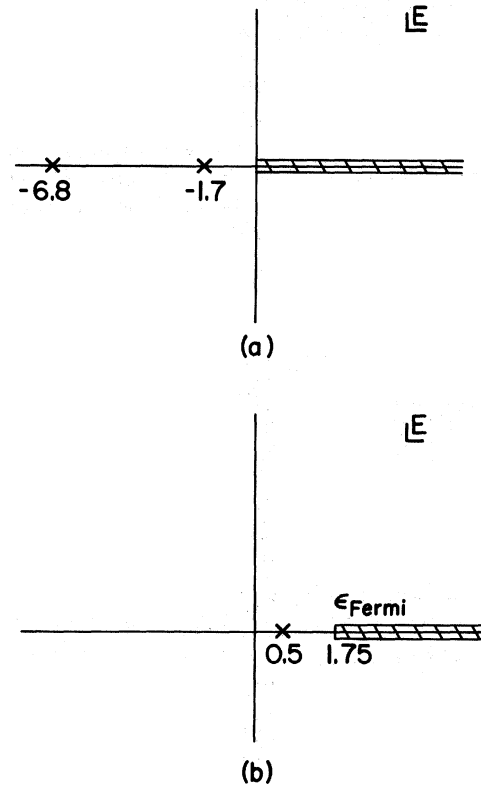


FIG. 11. (a) Analytic structure of the Bethe-Goldstone solution $t_{ep}^{\text{BG}}(E)$ along the real-energy axis in the zero-density limit. The pole at -6.8 eV corresponds to the positronium ground state. There are also an infinite number of poles in the interval $-1.7 \text{ eV} < E < 0$ which for reasons of clarity we do not attempt to show. (b) Analytic structure of $t_{ep}^{\text{BG}}(E)$ at $r_s = 7.6$. Note the nonzero threshold at $+1.75 \text{ eV}$, and the pole on the positive real-energy axis at $+0.5 \text{ eV}$.

For simplicity we have chosen $\vec{K} = 0$, corresponding to the annihilation of a positron with an electron at the bottom of the Fermi sea, but the threshold remains nonzero even in the other extreme in which the stationary positron annihilates with an electron at the top of the Fermi sea and $|\vec{K}| = k_F$. Then,

$$E_{\text{thresh}} = (k_F - |\frac{1}{2}\vec{K}|)^2 = \frac{1}{4}k_F^2 > 0. \quad (42)$$

The positive-energy cut extends from infinity to the branch point at $E_{\text{thresh}} > 0$, and this causes the difficulties. The position of the 1S bound state pole of $t_{ep}^{\text{BG}}(E)$ as a function of density is shown in Fig. 12(a). For $r_s > 8.4$ the position of this pole agrees with the calculations of Held and Kahana²⁷ and Arponen.²⁸ However, these papers failed to note that at $r_s = 8.4$ the pole crosses over

from the negative real E axis to the positive real E axis. This can occur because the threshold branch point is no longer at the origin but at $E = E_{\text{thresh}} > 0$, Fig. 11(b). If we further increase the density, the pole approaches E_{thresh} asymptotically but never reaches it, so that it exists for arbitrarily high density and for an arbitrarily weak interaction. The magnitude of the bound-state wave function at $r = 0$, $|\psi^{\text{BG}}(r=0)|^2$, is shown as a function of r_s in Fig. 12(b). Since it is normalized,

$$\int |\psi^{\text{BG}}(\vec{r})|^2 d^3r = 1, \quad (43)$$

this again provides us with a measure of the degree of localization of the bound state. As the density increases, $|\psi^{\text{BG}}(r=0)|^2$ tends only asymptotically to zero, so that the bound state becomes arbitrarily diffuse but always exists. The mechanism acting here is very similar to the one which generates Cooper bound-state pairs for arbitrarily weak attraction in the presence of a Fermi sea, in the BCS theory of superconductivity.²⁹

As an example of the effect of a nonzero threshold for an attractive interaction, consider the exactly soluble model of a separable potential,

$$\langle \vec{p} | V_{\text{sep}} | \vec{k}_0 \rangle = (2\pi^2\lambda) \tilde{v}(|\vec{p}|) \tilde{v}(|\vec{k}_0|), \quad \lambda < 0. \quad (44)$$

The Bethe-Goldstone equation with this potential has the exact solution

$$\langle \vec{p} | t_{\text{sep}}^{\text{BG}}(E) | \vec{k}_0 \rangle = \frac{(2\pi^2\lambda) \tilde{v}(|\vec{p}|) \tilde{v}(|\vec{k}_0|)}{1 + \lambda \int_{k_F}^{\infty} dq q^2 [\tilde{v}^2(|\vec{q}|)/(q^2 - E)]}. \quad (45)$$

For $k_F > 0$ and any $\lambda < 0$, $t_{\text{sep}}^{\text{BG}}(E)$ always has a pole at some real $E < k_F^2$, since the integral covers all non-negative values as E varies from $-\infty$ to k_F^2 . However, if $k_F = 0$ the integral has an upper bound, since the phase-space factor q^2 cancels with the pole at $E = 0$. Then $t_{\text{sep}}^{\text{BG}}(E)$ has a pole on the real E axis only if the attraction is sufficiently strong:

$$\lambda < - \left[\int_0^{\infty} dq \tilde{v}^2(|\vec{q}|) \right]^{-1}. \quad (46)$$

This exact example illustrates two important points. For nonzero threshold (i) poles can exist at positive energies, and (ii) these poles will continue to exist for arbitrarily weak attraction.

Returning to the present calculation, we find that the Bethe-Goldstone equation generates a bound state embedded in the positive-energy continuum states, for the entire range of metallic densities $2 \leq r_s \leq 6$. We know that the Bethe-Goldstone wave functions are not orthogonal to each other, so there will be components of this bound-state wave function in all the continuum states, and not just in the continuum state which is de-

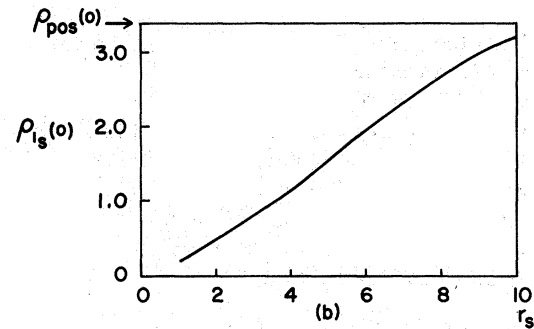
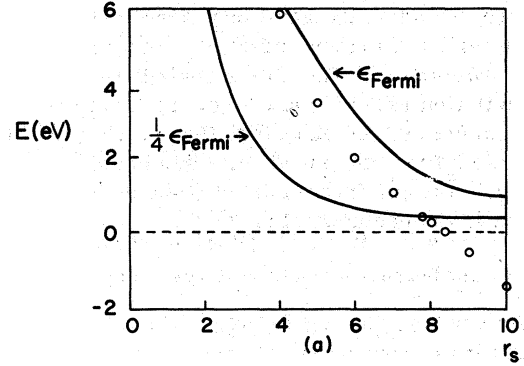


FIG. 12. (a) Small circles indicate position of the $1S$ bound-state pole for the Bethe-Goldstone solution $t_{\text{sep}}^{\text{BG}}(E)$. The curve ϵ_{Fermi} is the energy threshold for physical scattering. The annihilation rate for the continuum states is averaged over $0 \leq E \leq \frac{1}{4}\epsilon_{\text{Fermi}}$, and for $7.8 < r_s < 8.4$ the bound-state pole lies within this region. (b) Electron density at positron site for $1S$ Bethe-Goldstone bound state. This measures the degree of localization of the state. Compare this with Fig. 10(b).

generate with the bound state. If we incorrectly apply plane-wave continuum normalization to a bound state, its contribution to annihilation rates is clearly divergent. This is the reason for the divergence in the Bethe-Goldstone rates. Since the positron is at rest, the initial relative momentum of the scattered positron electron is $\vec{k}_0 = \frac{1}{2}|\vec{k}_e - \vec{k}_p|$, i.e., $0 \leq |\vec{k}_0| \leq \frac{1}{2}k_F$. The rate must thus be averaged only over those continuum states for which $0 \leq E \leq \frac{1}{4}k_F^2 = \frac{1}{4}\epsilon_{\text{Fermi}}$ [see Fig. 12(a)]. At high densities the bound-state pole is very close to ϵ_{Fermi} and far away from the averaging region because of the kinematic constraints. For this reason, at high densities the Bethe-Goldstone rate is finite and, coincidentally, is in good agreement with the experimental rates. As the density decreases, the bound-state pole moves away from ϵ_{Fermi} and towards the region $0 \leq E \leq \frac{1}{4}\epsilon_{\text{Fermi}}$. By $r_s = 5$, components of the bound state are significantly mixing with the continuum states in this

region. At $r_s = 7.8$, the pole itself moves into the region, and the bound-state components diverge since they are incorrectly given continuum normalizations.

We may show this divergence is indeed a result of incorrect normalization coupled with the mixing of continuum and bound states, by defining a modified continuum wave function $|\bar{\psi}_E\rangle$ in which the bound-state wave function $|\psi_{E_B}\rangle$ has been projected out,

$$|\bar{\psi}_E\rangle \equiv (1 - |\psi_{E_B}\rangle\langle\psi_{E_B}|)|\psi_E\rangle. \quad (47)$$

We find $\langle\psi_{E_B}|\psi_E\rangle \neq 0$ even when $E \neq E_B$ confirming that the continuum and bound states are not orthogonal. Also we find that $\langle\bar{\psi}_E|\psi_E\rangle$ does not diverge for $r_s > 5$ but in fact decreases smoothly toward the noninteracting wave function. Thus, simply projecting out the bound-state wave function from the continuum wave functions removes the divergence. This pinpoints the cause of the divergence. If, without further justification, we add the separate rates from the modified continuum wave functions $|\bar{\psi}_E\rangle$ and the bound-state wave functions $|\psi_{E_B}\rangle$,

$$R = \frac{1}{4} \frac{R_{Ps}}{|\Phi_{Ps}(r=0)|^2} \left(\frac{1}{\frac{4}{3}\pi(r_s a_0)^3} \times \sum_{E < \frac{1}{2} k_F^2} |\langle\bar{\psi}_E|\psi_E\rangle|^2 + |\langle\psi_{E_B}|\psi_E\rangle|^2 \right), \quad (48)$$

we find that this rate is very close to the rate computed by Bhattacharyya and Singwi,¹⁹ curve c of Fig. 1, over the whole metallic density range $2 \leq r_s \leq 6$.

We would like to re-emphasize that the Bethe-Goldstone equation does not correctly antisymmetrize the electron wave functions, so that the results from this artificial separation have no physical significance. They serve only to unambiguously locate the cause of the divergences in the Bethe-Goldstone rates found in previous calculations. We conclude that the divergence is due to the mismatch of normalizations, resulting from an unphysical mixing of continuum and bound-state wave functions. The mixing is caused by using the Bethe-Goldstone equation in a problem for which it is not applicable because the positron is an impurity.

V. RESULTS FOR POSITRON ANNIHILATION AND CONCLUDING REMARKS

Our computed rates for positron annihilation with valence electrons are shown in Fig. 13. We also show the experimentally observed rates in the alkali metals^{34,35} and in aluminum.³⁰⁻³⁴ Our rates are slightly higher than the observed rates.

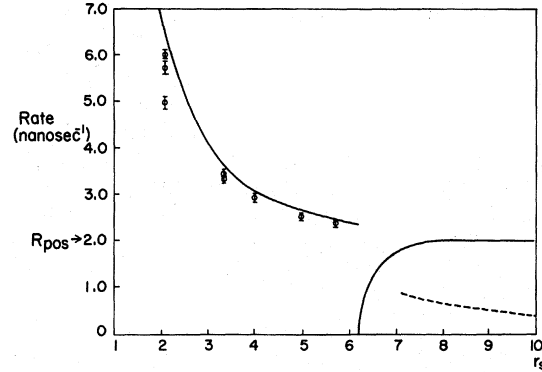


FIG. 13. Positron-annihilation rates in nsec^{-1} for our calculation. Experimental points from left to right are for Al (Refs. 30-34), Li, Na, K (Refs. 34 and 35), and Cs (Ref. 34). For $r_s > 6.2$, the solid line is the contribution to the rate from the $1S$ bound state, and the broken line is the approximate contribution to the rate from the continuum states.

Since our calculations were made for positron annihilation in the electron gas, we should compare our calculated rates to the experimental rates only after effects of the lattice as well as annihilations with core electrons have been subtracted out. If we were to simply subtract Carbotte and Salvadori's¹⁵ estimates of the annihilation rate with core electrons for aluminum and sodium the results would be 20% smaller than our calculated rates, but lattice effects could greatly reduce this difference.

There are some identifiable terms we have neglected which would tend to lower our rates. In our $V_{\text{eff}}^{(1)}$ we assumed complete cancellation of direct and exchange diagrams for momentum transfers greater than the cutoff momentum k_F . Since the exchange terms actually only cancel to leading order, this assumption will underestimate the screening, and hence overestimate the rate. Similarly, referring to our arguments about the three-particle bound state in Sec. IV, we would expect terms we have neglected of higher order in t_{ep} and t_{ee} (Fig. 9), would further increase the screening and lower the rates. We also found that our RPA self-energy insertions significantly lowered the rates, so that a more sophisticated treatment of self-energies is probably necessary.

With that said, the agreement with the observed rates is still remarkably good over the entire range of metallic densities. For $r_s > 4$ our rates continue to decrease smoothly toward the free positronium rate of 2.0 nsec^{-1} in marked contrast to the Bethe-Goldstone rates. At $r_s = 6.2$ the $1S$ bound state is formed and, by $r_s = 7$, its contribution to the rate is already 1.8 nsec^{-1} . With the

approximations discussed in Sec. IV, the continuum contributions to the rate for $r_s > 6.2$ decrease toward the rate for a noninteracting positron as expected. Thus, this approach may also be useful for the description of positron annihilation at the lower electron densities which would occur in the vicinity of a lattice defect, a negative-ion impurity, or the surface of a metal.

ACKNOWLEDGMENTS

The authors gratefully acknowledge many helpful discussions with Dr. S. O. Bäckman, Professor G. E. Brown, Dr. V. Emery, and Dr. S. Kahana.

APPENDIX: SELF-ENERGIES

The single-particle energy for a positron or an electron with momentum \vec{k} and self-energy insertions $\Sigma^{(e,p)}$ is

$$\epsilon_{\pm}(\vec{k}) = \frac{1}{2}|\vec{k}|^2 + \Sigma^{(e,p)}(\vec{k}, \epsilon_{\pm}(\vec{k})), \tag{A1}$$

where (e) or (p) labels the particle as an electron or a positron. The Hartree self-energy for either type of particle is exactly cancelled by the particle interaction with the uniform positive background, Fig. 14(a). Since the density of positrons in the metal is very low, the exchange part of the Hartree-Fock self-energy is only significant for the electron, Fig. 14(b). This may be included in the RPA self-energy term which is defined as [Fig. 14(c)],

$$\Sigma_{\text{RPA}}^{(e)}(\vec{k}, \omega) = \frac{1}{(2\pi)^4} \int d^3k' \int d\omega' e^{-i\eta\omega'} \times \frac{V(\vec{k}')}{1 - \Pi_0(\vec{k}', \omega')V(\vec{k}')} G_0^{(e)}(\vec{k} - \vec{k}', \omega - \omega'), \tag{A2}$$

$$\Sigma_{\text{RPA}}^{(p)}(\vec{k}, \omega) = \frac{1}{(2\pi)^4} \int d^3k' \int d\omega' e^{-i\eta\omega'} \times \frac{V(\vec{k}')\Pi_0(\vec{k}', \omega')V(\vec{k}')}{1 - \Pi_0(\vec{k}', \omega')V(\vec{k}')} G_0^{(p)}(\vec{k} - \vec{k}', \omega - \omega'),$$

where

$$G_0^{(e)}(\vec{k}, \omega) = i/[\omega - \frac{1}{2}k^2 + i\eta \operatorname{sgn}(|\vec{k}| - k_F)], \quad \eta = 0^+ \tag{A3}$$

$$G_0^{(p)}(\vec{k}, \omega) = i/(\omega - \frac{1}{2}k^2 + i\eta), \quad \eta = 0^+$$

$$\epsilon_{\pm}(\vec{k}) \simeq \frac{1}{2}|\vec{k}|^2 + \Sigma_{\text{RPA}}^{(e,p)}(\vec{k}, \frac{1}{2}|\vec{k}|^2) + [\epsilon_{\pm}(\vec{k}) - \frac{1}{2}|\vec{k}|^2] \left. \frac{\partial \Sigma_{\text{RPA}}^{(e,p)}(\vec{k}, \omega)}{\partial \omega} \right|_{\omega = |\vec{k}|^2/2}$$

$$= \frac{1}{2}|\vec{k}|^2 + \Sigma_{\text{RPA}}^{(e,p)}(\vec{k}, \frac{1}{2}|\vec{k}|^2) \left/ \left(1 - \frac{\partial \Sigma_{\text{RPA}}^{(e,p)}(\vec{k}, \omega)}{\partial \omega} \right) \right|_{\omega = |\vec{k}|^2/2}. \tag{A4}$$

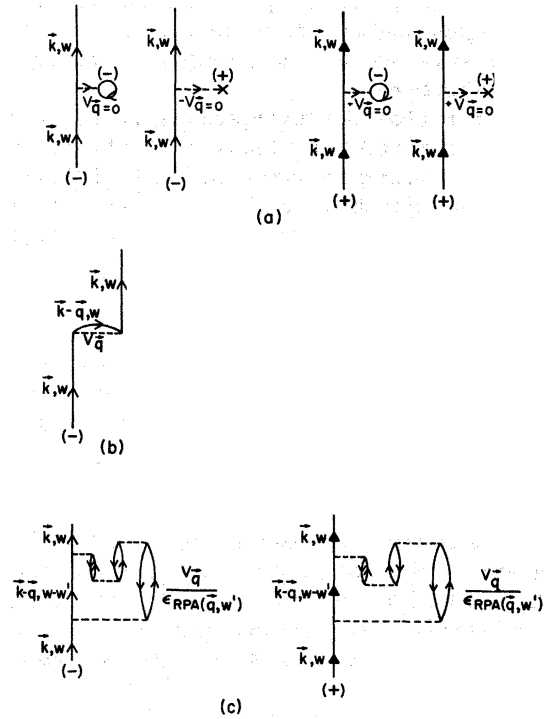


FIG. 14. (a) Hartree self-energy exactly cancels interaction with uniform positive background for both positron and electron. (b) Exchange part of Hartree-Fock self-energy for electron. For positron this term is negligible. (c) RPA self-energy insertion for positron and electron.

are the free-electron and positron Green's functions. For small $|\vec{k}|$, $\Sigma_{\text{RPA}}^{(e,p)}(\vec{k}, \epsilon_{\pm}(\vec{k}))$ should be a good approximation to the self-energy insertions. For large $|\vec{k}|$ the self-energy effects should be small, because the uncertainty principle restricts the time available for the original virtual excitation of momentum \vec{k} to produce additional virtual excitations in self-energy-type processes.³⁶ Since $\Sigma_{\text{RPA}}^{(e,p)}(\vec{k}, \epsilon_{\pm}(\vec{k}))$ itself goes quite rapidly to zero for $|\vec{k}| > 1.5k_F$, we used it to approximate self-energy effects for all \vec{k} , regarding it as an interpolating function between the high- and low- $|\vec{k}|$ limits.

We used the techniques developed by Hedin³⁷ to calculate $\Sigma_{\text{RPA}}^{(e)}(\vec{k}, \frac{1}{2}|\vec{k}|^2)$ and extended them to calculate $\Sigma_{\text{RPA}}^{(p)}(\vec{k}, \frac{1}{2}|\vec{k}|^2)$. To relate $\Sigma_{\text{RPA}}(\vec{k}, \frac{1}{2}|\vec{k}|^2)$ to $\Sigma_{\text{RPA}}(\vec{k}, \epsilon_{\pm}(\vec{k}))$, we used the Taylor expansion, to first order,

- *Research supported in part by U. S. Atomic Energy Commission Contract No. AT(11-1)-3001.
- †Present address: Physics Dept., Northwestern University, Evanston, Ill. 60201.
- ¹D. N. Lowy and G. E. Brown, Phys. Rev. B (to be published).
- ²For recent reviews see I. Ya. Dekhtyar, Phys. Rep. C 9, 243 (1974); A. Seeger, J. Phys. F 3, 248 (1973). R. N. West, Adv. Phys. 22, 263 (1973).
- ³R. E. Bell and R. L. Graham, Phys. Rev. 90, 644 (1953).
- ⁴R. A. Ferrell, Rev. Mod. Phys. 28, 308 (1956).
- ⁵G. Lee-Whiting, Phys. Rev. 97, 1557 (1955).
- ⁶J. P. Carbotte and H. L. Arora, Can. J. Phys. 45, 263 (1967).
- ⁷S. Kahana, Phys. Rev. 129, 1622 (1963).
- ⁸J. P. Carbotte and S. Kahana, Phys. Rev. 139, A213 (1965).
- ⁹B. Bergersen, Ph.D. thesis (Brandeis University, 1964) (unpublished); J. P. Carbotte, Phys. Rev. 155, 197 (1967).
- ¹⁰A. J. Zuchelli and T. G. Hickman, Phys. Rev. 136, A1728 (1964).
- ¹¹J. Crowell, V. E. Anderson, and R. H. Ritchie, Phys. Rev. 150, 243 (1966).
- ¹²J. Arponen and P. Jauho, Phys. Rev. 167, 239 (1968).
- ¹³H. Kanazawa, Y. Hotsuki, and S. Yanagawa, Prog. Theor. Phys. 33, 1010 (1965).
- ¹⁴B. B. J. Hede and J. P. Carbotte, J. Phys. Chem. Solids 33, 727 (1972).
- ¹⁵J. P. Carbotte and A. Salvadori, Phys. Rev. 162, 290 (1967); J. P. Carbotte, Phys. Rev. 144, 309 (1966).
- ¹⁶R. N. West, Solid State Commun. 9, 1417 (1971).
- ¹⁷F. H. Geisler, K. G. Lynn, and A. N. Goland (private communication).
- ¹⁸A. Sjölander and M. J. Stott, Phys. Rev. B 5, 2109 (1972).
- ¹⁹F. Bhattacharyya and K. S. Singwi, Phys. Rev. Lett. 29, 22 (1972).
- ²⁰K. S. Singwi, M. P. Tosi, R. H. Land, and A. Sjölander, Phys. Rev. 176, 589 (1968), referred to as STLS.
- ²¹P. Vashishta and K. S. Singwi, Phys. Rep. C 9, 875 (1972).
- ²²K. S. Singwi (private communication).
- ²³A. L. Fetter and J. D. Walecka, *Quantum Theory of Many-Particle Systems* (McGraw-Hill, New York, 1971).
- ²⁴K. L. Kowalski, Phys. Rev. Lett. 15, 798 (1965).
- ²⁵F. E. Low, *The Quantum Theory of Scattering* (Brandeis U.P., Waltham, Mass., 1959).
- ²⁶B. B. J. Hede and J. P. Carbotte, Can. J. Phys. 60, 1756 (1972); H. Yasuhara, J. Phys. Soc. Jpn. 36, 361 (1974).
- ²⁷A. Held and S. Kahana, Can. J. Phys. 42, 1908 (1964).
- ²⁸J. Arponen, J. Phys. C 3, 107 (1970).
- ²⁹L. N. Cooper, Phys. Rev. 104, 1189 (1956).
- ³⁰I. K. MacKenzie, T. L. Khoo, A. B. McDonald, and B. T. A. McKee, Phys. Rev. Lett. 19, 946 (1967).
- ³¹P. Hautojärvi, A. Tamminen, and P. Jauho, Phys. Rev. Lett. 24, 459 (1970).
- ³²B. T. A. McKee, A. G. D. Jost, and I. K. MacKenzie, Can. J. Phys. 50, 415 (1972).
- ³³R. M. J. Cotterill, K. Petersen, G. Trumpy, and J. Träff, J. Phys. F 2, 459 (1972).
- ³⁴H. Weisberg and S. Berko, Phys. Rev. 154, 249 (1967).
- ³⁵I. K. MacKenzie, T. W. Craig, and B. T. A. McKee, Phys. Lett. A 36, 227 (1971).
- ³⁶G. E. Brown, in *Methods and Problems of Theoretical Physics*, edited by J. E. Bowcock (North-Holland, Amsterdam, 1970).
- ³⁷L. Hedin, Phys. Rev. 139, A796 (1965).